WARSAW UNIVERSITY OF TECHNOLOGY Index 351733
FACULTY OF CIVIL ENGINEERING
COMMITTEE FOR CIVIL AND WATER ENGINEERING
POLISH ACADEMY OF SCIENCES ISSN 1230-2945
DOI: 10.24425/ace.2024.148913
ARCHIVES OF CIVIL ENGINEERING
Vol. LXX ISSUE 1 2024
pp. 305 –323

© 2024. Maria Kowalska, Janina Zaczek-Peplinska, Łukasz Piasta.

This is an open-access article distributed under the terms of the Creative Commons Attribution-NonCommercial-NoDerivatives License (CC BY-NC-ND 4.0, https://creativecommons.org/licenses/by-nc-nd/4.0/), which permits use, distribution, and reproduction in any medium, provided that the Article is properly cited, the use is non-commercial, and no modifications or adaptations are made.

Research paper

Determining the trend of geometrical changes of a hydrotechnical object based on data in the form of LiDAR point clouds

Maria Kowalska[1], Janina Zaczek-Peplinska[2], Łukasz Piasta[3]

Abstract: Monitoring the technical condition of hydrotechnical facilities is crucial for ensuring their safe usage. This process typically involves tracking environmental variables (e.g., concrete damming levels, temperatures, piezometer readings) as well as geometric and physical variables (deformation, cracking, filtration, pore pressure, etc.), whose long-term trends provide valuable information for facility managers. Research on the methods of analyzing geodetic monitoring data (manual and automatic) and sensor data is vital for assessing the technical condition and safety of facilities, particularly when utilizing new measurement technologies. Emerging technologies for obtaining data on the changes in the surface of objects employ laser scanning techniques (such as LiDAR, Light Detection, and Ranging) from various heights: terrestrial, unmanned aerial vehicles (UAVs, drones), and satellites using sensors that record geospatial and multispectral data. This article introduces an algorithm to determine geometric change trends using terrestrial laser scanning data for both concrete and earth surfaces. In the consecutive steps of the algorithm, normal vectors were utilized to analyze changes, calculate local surface deflection angles, and determine object alterations. These normal vectors were derived by fitting local planes to the point cloud using the least squares method. In most applications, surface strain and deformation analyses based on laser scanning point clouds primarily involve direct comparisons using the Cloud to Cloud (C2C) method, resulting in complex, difficult-to-interpret deformation maps. In contrast, preliminary trend analysis using local normal vectors allows for rapid threat detection. This approach significantly reduces calculations, with detailed point cloud interpretation commencing only after detecting a change on the object indicated by normal vectors in the form of an increasing deflection trend. Referred to as the cluster algorithm by the authors of this paper, this method can be applied to monitor both concrete and earth objects, with examples of analyses for different object types presented in the article.

Keywords: LiDAR, normal vectors, point clouds, terrestrial laser scanning, deformations of hydrotechnical structures, cluster algorithm

[1]PhD, Warsaw University of Technology, Faculty of Geodesy and Cartography, pl. Politechniki 1, 00-661 Warsaw, Poland, e-mail: maria.kowalska@pw.edu.pl, ORCID: 0000-0003-0058-0976
[2]PhD, Warsaw University of Technology, Faculty of Geodesy and Cartography, pl. Politechniki 1, 00-661 Warsaw, Poland, e-mail: Janina.peplinska@pw.edu.pl, ORCID: 0000-0003-4875-4250
[3]MSc, Warsaw University of Technology, Faculty of Geodesy and Cartography, pl. Politechniki 1, 00-661 Warsaw, Poland, e-mail: Lukasz.piasta@pw.edu.pl

1. Introduction

Monitoring the technical condition of hydrotechnical structures is critical for ensuring their safe usage. Over the years, it has been performed using various geodetic and geotechnical techniques. Digital advancements have yielded new techniques and sensors for displacement monitoring, capable of overcoming the limitations of traditional instruments such as tachymeters and precision levels [1]. Hydrotechnical measurements increasingly rely on digital photogrammetry, 2D image correlation methods (2D DIC), particle image velocimetry (PIV), unmanned aerial vehicles (UAVs), and terrestrial laser scanning (TLS) [2]. These techniques enable the acquisition of high-resolution point clouds over a large surface area in a short time and without direct contact with the structure. The acquired point cloud data facilitate various types of analyses: precise imaging of changes on the structure in the form of difference maps and cross-sections conducted at selected locations of the structure according to the designer's guidelines and risk assessment needs. In terms of applicability, photogrammetry, and PIV are more suitable for close-range measurements on a small scale [2, 3], while UAVs are commonly used in inventories and displacement measurements of dams [2, 4, 5] and embankments [6]. Mobile LiDAR [7] data are also utilized for monitoring flood embankments, enabling rapid measurements with an accuracy of a few centimeters. TLS technology allows for centimeter-level accuracy measurements and when maintaining an appropriate measuring regime, even millimeter-level accuracy, thus being employed not only in inventories but also in high-precision work [2]. In the past decade, numerous researchers have illustrated the usefulness of TLS for detecting deformations in concrete water dams [8, 11] and applying TLS for monitoring concrete, earthen, and embankment dams [3].

All the aforementioned measurement techniques are compared, combined, and utilized in interdisciplinary monitoring projects. For example, the paper by Bolkas presented an evaluation and comparison of sUAS photogrammetry and TLS technologies at the Francis E. Walter Dam in northeast Pennsylvania. TLS accuracy levels are considered sufficient for year-to-year monitoring of earth-filled embankment dams where smaller displacements are expected (e.g., 5.0–14.0 cm per year), while the sUAS accuracy level is more suitable for 5–10-year intervals where larger displacements are expected (e.g., about 40.0 cm) [12]. Another example is the integration of these technologies into comprehensive monitoring solutions. For instance, Kang et al. investigated the possibility of determining settlements as an element of dam body maintenance assessment using UAV structure from motion (UAV-SfM) and TLS point clouds [13].

In this article, we present a clustering algorithm that allows the determination of surface geometry change trends based on normal vectors calculated from terrestrial laser scanning data for both concrete and earthen surfaces.

Many authors have discussed the use of terrestrial laser scanning for periodic, rather than continuous, monitoring of water barriers [9]. In one article, Italian researchers employed the TLS technique to measure the displacements of a water dam on Lake Cancano. By mutually aligning previously generated triangle irregular network (TIN) grids and object models for dam point clouds from different measurement periods, they developed differential models to assess the geometry of concrete dam section deformations. However, such labor-intensive

model development methods are unsuitable for automatic monitoring, where risk areas should be identified in real-time or shortly after a single control measurement series.

In most described applications of point clouds obtained from various LiDAR systems, surface deformation, and strain analyses are based on direct point distance comparisons, such as the Cloud to Cloud (C2C) method. This generates extensive deformation maps that can be difficult to interpret. The adopted color scale and deformation range of these maps can lead to varying conclusions about an object's behavior. Proper analysis demands focus and experience to select genuinely significant information from a vast amount of data and avoid subjective evaluations.

As automatic object monitoring systems require clear answers regarding whether a change has occurred, we propose an easy-to-implement algorithm that divides the point cloud into fields, numerically determining the maximum change. Field dimensions should correlate with the expected change size. While there can be multiple approaches to determining the maximum change value for a point cloud fragment, it is crucial to focus on actual change or deformation. Point clouds inherently depict not only deformations but also measurement noise and local surface roughness. Consequently, determining the trend of changes based on such datasets should not solely rely on calculating distances between cloud points (point to point, P2P).

This article suggests a preliminary trend analysis of the object's behavior, utilizing local normal vectors for rapid threat detection, regardless of surface roughness and measurement noise. This approach provides information about the occurrence of changes and significantly reduces the number of calculations. If the structure shows no changes, detailed point cloud analysis commences only after detecting a change on the structure, indicated by normal vectors in the form of an increasing deflection trend.

Hyungjoon Seo also used normal vectors to identify changes, applying the P2P-TA comparison method, which calculates the tilt angle from normal vectors of planes simulated from point clouds [14]. He observed that laser scanning could evaluate the global behavior of an entire retaining structure, though the accuracy was insufficient for detailed analysis. However, the author highlighted the method's considerable potential with proper data acquisition. Normal vectors offer numerous applications in point cloud analysis [15], and that is why the authors of this paper propose their use for detecting the occurrence of surface deformation in various structures.

2. Methods

As mentioned in the introduction, the developed algorithm, named the cluster algorithm by the authors, uses normal vectors of fitted planes in point cloud fragments to determine the maximum changes on the object. The algorithm is divided into 8 basic steps and is presented in Fig. 1.

In the first step, the cluster algorithm divides the point clouds from the reference measurement (structure before the change) and the subsequent one (performed to identify potential changes) into squares. If it is not possible to achieve only regular square-shaped fields, it is recommended to separate the maximum number of squares and rectangles from the remaining

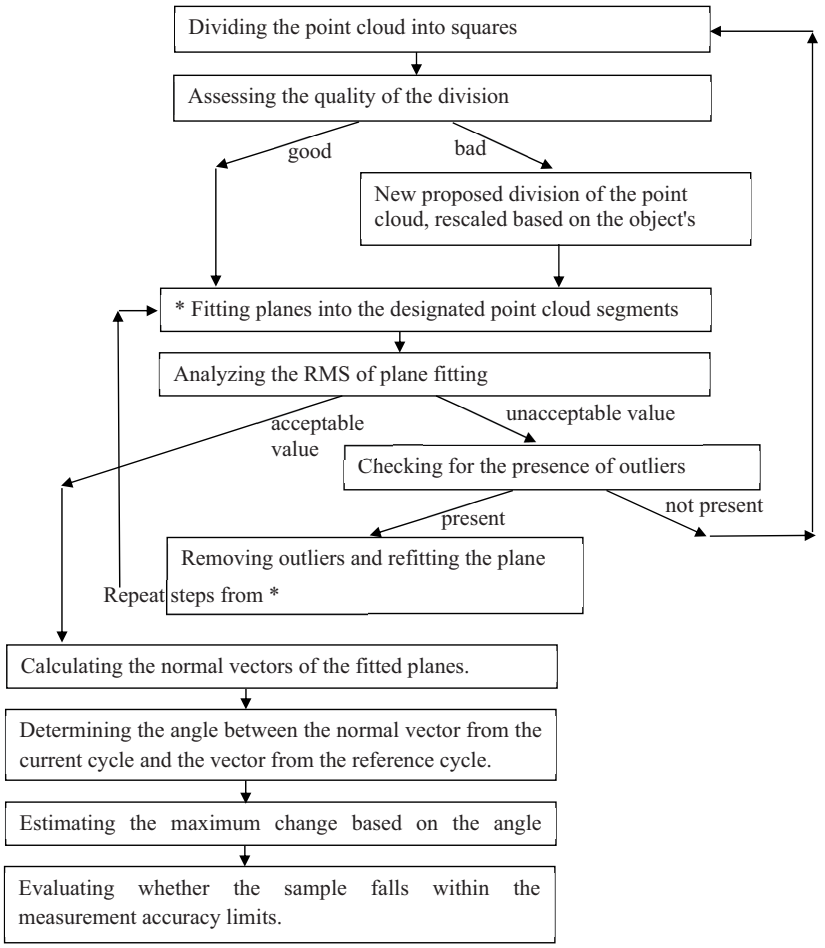

Fig. 1. The consecutive steps of the cluster algorithm for determining maximum changes based on point clouds

part of the point cloud. The basis for choosing the dimensions of the squares is the vertical and horizontal dimensions of the scanned surface, as well as its type and the expected change value. For flat, smooth surfaces, where we expect, for example, deflections, we can apply larger squares than for rough, undulating surfaces, where changes occur suddenly and randomly. Auxiliary parameters for selecting square sizes may be the surface roughness parameters Ra and Rz determined for the entire scanned surface. Measurement in IMSGeo is based on a defined measurement log, which determines the planned number of measured points in rows and columns, which is a significant facilitation in planning the division of the point cloud.

In the second step, the quality of the division is assessed. The basic criterion is to verify the number of points in the separated areas. The number of registered points may vary due to discontinuities on the object's surface, such as windows in a building – empty fields without

measured points, surfaces from which the laser beam was not reflected, or erroneous point measurement to an obscuring object or other terrain obstacle. Considering the impact of the number of points on the quality of determining the change, it is recommended that the number of points in the squares be above 75% of the theoretical number of points, assuming that the entire square is filled with data. Otherwise, a decision should be made on a new division of the point cloud, rescaled based on the object's proportions.

In the third step, planes are fitted into the separated fragments of point clouds. The plane fitting is done using the least squares method. The plane is described by the normal vector $n = [a, b, c]^T$ and the distance d, so for the point $P = [x, y, z]^T$ on the plane, $n \cdot p + d = 0$. The formula for calculating the plane (Eq. 2.1) parameters is:

$$ax + by + cz + d = 0 \tag{2.1}$$

assuming that $c = 1$, we obtain:

$$ax + by + z + d = 0 \tag{2.2}$$

$$ax + by + d = -z \tag{2.3}$$

For a set of points, the matrix form of the equation (Eq. 2.4) is:

$$\begin{bmatrix} x_0 & y_0 & 1 \\ \dots & \dots & \dots \\ x_n & y_n & 1 \end{bmatrix} \begin{bmatrix} a \\ b \\ d \end{bmatrix} = \begin{bmatrix} -z_0 \\ \dots \\ -z_n \end{bmatrix} \tag{2.4}$$

Where n is the number of points.

(2.5)

$$\begin{bmatrix} x_0 & x_1 & \dots & x_n \\ y_0 & y_1 & \dots & y_n \\ 1 & 1 & \dots & 1 \end{bmatrix} \begin{bmatrix} x_0 & y_0 & 1 \\ x_1 & y_1 & 1 \\ \dots & \dots & \dots \\ x_n & y_n & 1 \end{bmatrix} \begin{bmatrix} a \\ b \\ d \end{bmatrix} = \begin{bmatrix} x_0 & x_1 & \dots & x_n \\ y_0 & y_1 & \dots & y_n \\ 1 & 1 & \dots & 1 \end{bmatrix} \begin{bmatrix} -z_0 \\ -z_1 \\ \dots \\ -z_n \end{bmatrix}$$

As a result of the fitting, we obtain the root mean square (RMS – Eq. 2.6).

$$\text{RMS} = \sqrt{\frac{1}{N} \sum_{i=1}^{N} x^2} \tag{2.6}$$

where N is the number of points in the square, x is the orthogonal distance of the point from the fitted surface.

RMS values ought to correspond with anticipated change ranges, ideally being smaller than the expected change.

The fourth step in the procedure entails examining the RMS values associated with plane fitting in point clouds. In instances of notably large RMS values, it is essential to inspect for outliers within the square. To eliminate such points, a statistical outlier removal (SOR) filter can be employed, after which the plane is refitted to the filtered point cloud before returning to step 4.

During the fifth step, both the centroids of the areas and the normal plane vector values are ascertained. The equation representing a plane that passes through point P(x_0, y_0, z_0) and is perpendicular to the nonzero vector N = (A, B, C) takes the form A($x - x_0$) + B($y - y_0$) + C($z - z_0$) = 0. This equation is known as the normal equation of the plane. The square's centroid is calculated by averaging individual coordinates.

In the sixth step, the angle between the normal vector from the current analyzed measurement cycle and its corresponding normal vector from the reference cycle is determined. This angle is calculated using the following formula (Eq. 2.7):

$$\cos\alpha = \frac{n_{x1} \cdot n_{xb} + n_{y1} \cdot n_{yb} + n_{z1} \cdot n_{zb}}{\sqrt{n_{x1} \cdot n_{x1} + n_{y1} \cdot n_{y1} + n_{z1} n_{z1}} \cdot \sqrt{n_{xb} \cdot n_{xb} + n_{yb} \cdot n_{yb} + n_{zb} n_{zb}}} \tag{2.7}$$

where α denotes the desired angle, index 1 corresponds to the reference cycle, and index b represents the current cycle.

During the seventh step, the maximum expected change is established based on the angle between the vectors. The formula used to determine the change, contingent upon the type of measured surface, may or may not factor in the RMS of the plane fit. Further details are provided in the subsequent chapter.

Lastly, in the final step, an evaluation is conducted to ensure that the sample adheres to measurement accuracy limits, verifying that the determined change is not excessively large, which would indicate a procedural error. As with any automated approach, this algorithm necessitates expert oversight of the resulting outcomes. Key control elements of the algorithm include verifying that the normal vector is a unit vector and that the angle value α does not surpass 90°.

3. Results of cluster algorithms tests

The algorithm was tested on two experimental subjects: an artificially created slope of an embankment and a building wall on Okrzei Street in Warsaw. The surfaces of these objects resemble those of standard hydrotechnical structures, such as earth embankments or downstream walls of water dams. They present similar challenges and measurement difficulties. For the slope, these challenges include surface irregularities and changing vegetation throughout the year due to the growing season. For the concrete wall, they encompass the object's significant height, unfavorable laser beam incidence angles, surface irregularities, and relatively high surface roughness compared to the range of determined changes.

The rationale for testing the algorithm on the described examples is supported by Fig. 2. a photo of the downstream side of the Klimkówka dam (analogous to the slope surface) and Fig. 3. photos of the high downstream wall of the Pilchowice dam with a face made of stones separated by joints (analogous to an irregular, rough-surface wall).

Due to a lack of appropriate data from hydrotechnical structures in the form of point clouds from at least two measurement periods, we decided to analyze available data from objects similar in nature.

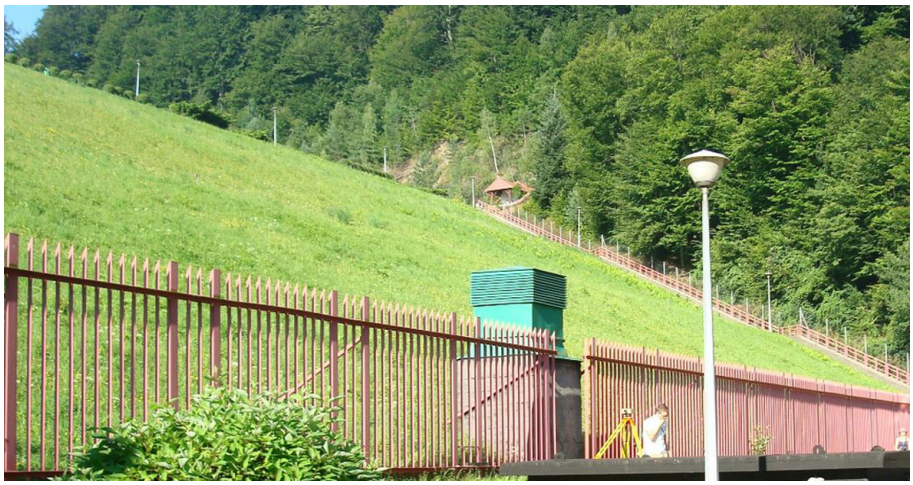

Fig. 2. The earth dam slope at Klimkówka in the summer period

(a) (b)

Fig. 3. Pilchowice dam wall: a) view of the wall with a visible ledge at the crown, b) surface structure of the wall

3.1. Slope

The first experimental subject, an earth slope, measures 26 meters in length and 7 meters in height. Two measurement cycles were conducted. The first cycle employed a point cloud from a ground-based laser scanner measurement, while the second used a point cloud obtained from digital photos captured by a DJI Phantom 4pro v2 drone (UAV) at a low altitude (30m). Earth embankments are increasingly monitored using terrestrial laser scanning (TLS) or UAVs, making the data selection in this experiment representative for hydrotechnical structure monitoring.

The slope was divided into 11 test fields. Ideally, the algorithm suggests dividing the area into squares. However, due to the object's atypical characteristics, incline, and non-linear edges, half of the designated fields are rectangular (Fig. 4). The division was considered suitable, and planes were fitted into individual fields. The plane fitting results for the first and second measurement cycles are presented as normal vector values, RMS, and centroid coordinates in Table 1 and Table 2, respectively. Both tables also display the parameters for fitting the plane to the entire point cloud and its marked fragment in Fig. 5.

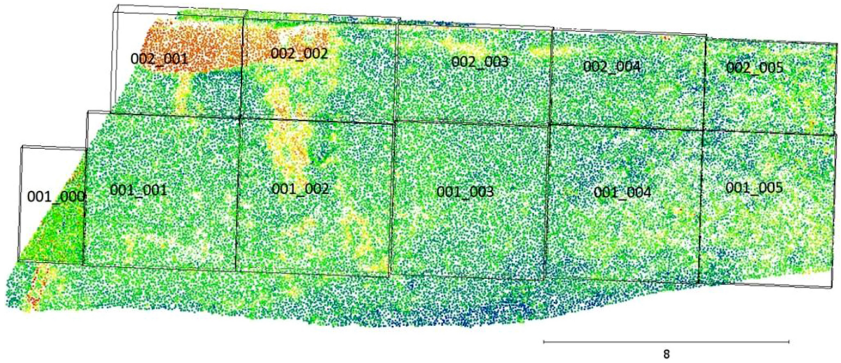

Fig. 4. View of the slope in intensity colors with the division into analyzed areas marked

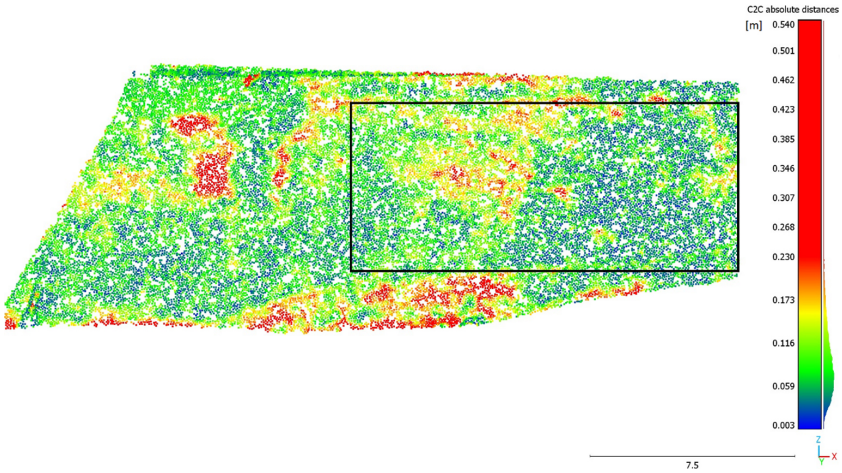

Fig. 5. Point cloud view of the slope in colors corresponding to the difference in point distances between cycles 1 and 2, determined by the C2C algorithm. A black frame indicates the slope fragment subjected to separate analyses

In both the first and second cycles, large RMS values (exceeding 0.10 m) were obtained for four out of 13 fittings. Caution should be exercised for fittings with high RMS values, and it should be verified whether any disturbances or noises are present in the point cloud that were not eliminated during the point cloud cleaning stage.

Based on the data in Tables 1 and 2, the angle sizes between normal vectors (α_N) and the distance between the initial vectors $N_{(sN1-N2)}$ were determined according to the following formula (Eq. 3.1).

$$\cos \alpha_N = \frac{\overrightarrow{N_1} \circ \overrightarrow{N_2}}{\left|\overrightarrow{N_1}\right| * \left|\overrightarrow{N_2}\right|} \tag{3.1}$$

where α_N is an angle between the normal vectors $\overrightarrow{N_1}$ and $\overrightarrow{N_2}$ for the cycle 1 and cycle 3, respectively.

The maximum size of the change for a given field was calculated based on the formula (Eq. 3.2):

$$\text{change } N = \text{length of the diagonal} \cdot \tan \alpha_N + s_{N1-N2} + \frac{(\text{RMS}_1 + \text{RMS}_2)}{2} \tag{3.2}$$

Due to the analysis of a sloped area with variable vegetation over time, it was decided to include the RMS average value in the N change formula. The obtained results were compared with the maximum expected change in the given field, determined earlier based on the C2C algorithm. The results are compiled in Table 3.

$$\text{agreement with the theoretical value} = \frac{\text{change } N}{\text{theoretical change max}} 100\% \tag{3.3}$$

Table 1. Compilation of normal vector values, root mean square (RMS), and centroid coordinates for planes fitted into the designated point cloud fragments representing the slope – cycle 1

ID	N_x	N_y	N_z	RMS [m]	RMS evaluation	X (p.N) [m]	Y (p.N) [m]	Z (p.N) [m]
001_000	0.2539	0.9668	–0.0283	0.02		194.51	765.86	26.51
001_001	0.0378	0.9992	0.0106	0.09		197.64	765.51	27.37
001_002	–0.1937	0.9806	–0.0282	0.08		202.49	765.94	27.51
001_003	–0.1068	0.9932	–0.0475	0.07		207.50	766.83	27.53
001_004	–0.0478	0.9988	–0.0078	0.07		212.50	767.21	27.51
001_005	–0.0258	0.9996	0.0077	0.06		217.06	767.37	27.53
002_001	–0.0120	0.8676	–0.4971	0.13	large	198.45	766.12	31.47
002_002	–0.0822	0.9164	–0.3918	0.15	large	202.49	766.55	31.67
002_003	–0.0719	0.9925	–0.0991	0.10	large	207.51	767.02	31.55
002_004	–0.0464	0.9986	–0.0241	0.08		212.50	767.23	31.51
002_005	–0.0156	0.9995	–0.0291	0.08		217.14	767.42	31.47
entire slope	–0.0831	0.9944	–0.0657	0.29	large	205.87	766.55	28.61
fragment	–0.0513	0.9987	–0.0047	0.08		212.24	767.16	28.93

Table 2. Compilation of normal vector values, root mean square, and centroid coordinates for planes fitted into the designated point cloud fragments representing the slope – cycle 2

ID	N_y	N_z	RMS [m]	RMS evaluation	X (p.N) [m]	Y (p.N) [m]	Z (p.N) [m]
001_000	0.9633	–0.0517	0.03		194.55	765.92	26.64
001_001	0.9992	–0.0133	0.09		197.68	765.59	27.37
001_002	0.9816	–0.0521	0.06		202.52	766.03	27.54
001_003	0.9911	–0.0448	0.04		207.50	766.92	27.49
001_004	0.9997	–0.0052	0.05		212.51	767.28	27.48
001_005	0.9996	0.0061	0.04		217.11	767.41	27.52
002_001	0.8811	–0.4713	0.11	large	198.41	766.22	31.43
002_002	0.9226	–0.3756	0.15	large	202.51	766.66	31.73
002_003	0.9907	–0.1124	0.10	large	207.51	767.13	31.55
002_004	0.9986	–0.0446	0.06		212.50	767.35	31.50
002_005	0.9993	–0.0327	0.04		217.14	767.48	31.46
entire slope	0.9944	–0.0674	0.29	large	205.87	766.65	28.66
fragment (Fig. 5)	0.9988	–0.0159	0.08		212.25	767.23	28.92

A satisfactory result is considered to agree with the theoretical value at the level of 100% ± 30%.

In Table 3, yellow marks fields for which no agreement was obtained at any level. These fields underwent analysis in search of outliers, and it was found that in the case of field 001_005, for which RMS in both measurement cycles did not exceed 10 cm, a specific situation occurred in which the surface shape was so symmetrical (Fig. 6) that the plane fitted into the point cloud was characterized by low RMS but was not representative of the change that occurred in the designated area. The determined change, in this case, was too small compared to the actual change. A similar situation occurred for field 002_005.

In the case of field 002_001, a surface fracture was found, which caused the fitted planes to be unrepresentative. In this case, the solution may be to divide the field into two parts along the surface fracture boundary and refit the planes. However, it should be emphasized that satisfactory results were obtained for 8 out of 11 fields, indicating the great potential of the method. Additionally, good results were obtained in both analysis variants: the entire slope and its fragment marked in Fig. 5. Moreover, Fig. 5. shows a map of differences in distances for individual points registered in cycle 1 and cycle 2. As can be seen in the figure, most changes exceeding 0.20;m occur locally and may be due to changing vegetation on the slope. Therefore, point-to-point (C2C) analyses are more challenging to interpret and do not allow for a quick determination of the changing trend.

Table 3. Compilation of the angle values between normal vectors, distances between the initial points of normal vectors, change values based on them, theoretical change values, and the agreement of the determined change with the theoretical change between cycle 1 and cycle 2

ID	α_N [g]	$s_{N_1-N_2}$ [m]	Change N [m]	Theoretical change max [m]	Agreement with theoretical change [%]
001_000	1.63	0.15	0.36	0.28	128.81
001_001	1.52	0.08	0.35	0.36	96.41
001_002	1.65	0.10	0.35	0.37	95.33
001_003	1.21	0.10	0.29	0.40	72.36
001_004	1.49	0.08	0.31	0.35	88.60
001_005	0.25	0.07	0.15	0.30	48.79
002_001	2.50	0.11	0.51	0.33	154.20
002_002	1.17	0.13	0.41	0.42	97.46
002_003	0.92	0.11	0.31	0.36	85.54
002_004	1.76	0.11	0.38	0.31	122.56
002_005	0.36	0.06	0.16	0.29	53.55
entire slope	0.15	0.11	0.42	0.53	79.63
fragment	0.76	0.07	0.24	0.26	92.46

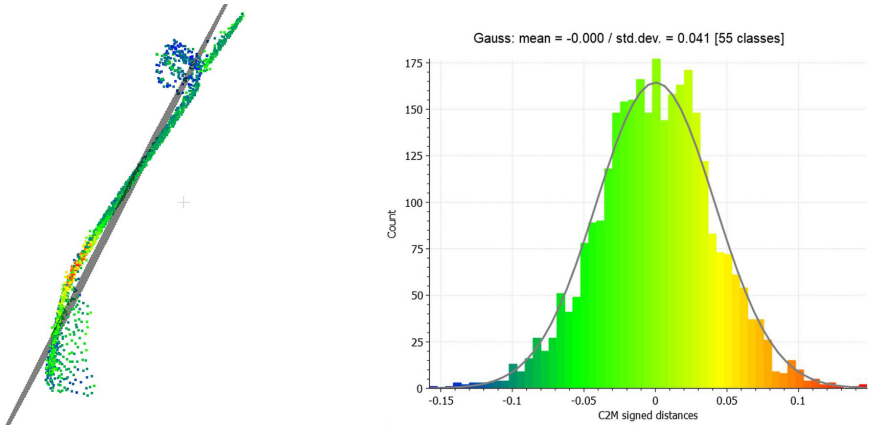

(a) (b)

Fig. 6. a) Point cloud view for field 001_005 cycle 2 with fitted plane b) distribution of point distances from the fitted plane for field 001_005 cycle 2, along with the fitted Gaussian normal distribution curve

The maximum changes on the slope surface determined by the proposed method oscillated within the range of 0.30–0.40 m. Figure 7 shows a histogram of the distances between points in cycle 1 and cycle 2, determined by the C2C algorithm. As can be seen on the chart, 99.7% of points have a change not exceeding 0.33 m, which is consistent with the results obtained based on normal vectors.

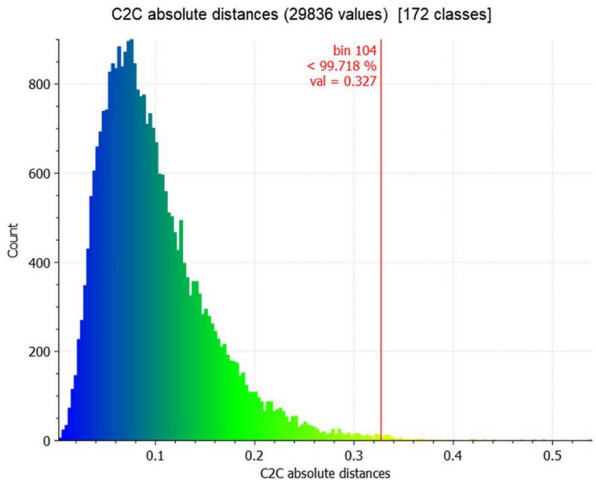

Fig. 7. Histogram of distance differences between points in cycle 1 and cycle 2 for the entire analyzed slope surface, determined by the C2C algorithm

3.2. Vertical wall – house at Okrzei Street

The second research object is a wall of a tenement house located on Stefana Okrzei Street in Warsaw. The analyzed surface was 20;m wide and 13;m high at its highest point. It was divided into 15 fields (Fig. 8), for which the maximum changes were determined using the presented cluster algorithm. The analyzed data came from two measurement cycles performed with the Leica MS60 scanning tachymeter.

Due to the irregular shapes of the structure, dividing the point cloud into square fields was significantly difficult. The main problem when dividing point clouds are all kinds of irregularities and faults. As shown in the earlier described example of an earth structure, data with significant surface irregularities do not allow for the correct determination of the change, hence when dividing the point cloud, it is necessary to check whether the designated fields approximately represent a plane. Data within the fields should be properly cleaned, and fields with a small amount of data or non-standard shape should be considered for rejection. In Table 4, fields that were rejected from the analysis were marked, and the values of normal vectors, root mean square, and coordinates of the centroid for planes fitted into the designated point cloud fragments representing the wall of the building on Stefana Okrzei Street in Warsaw – cycle 1 were summarized. In addition, the plane fitting analysis was performed for the entire point cloud (without division) and for its fragment in the original variant, and the variant was

Table 4. A summary of normal vector values, root mean square (RMS), and centroid coordinates for planes fitted to the designated point cloud segments representing the wall of the building on Stefana Okrzei Street in Warsaw – Cycle 1

ID	Notes	N_x	N_y	N_z	RMS [m]	X (p.N) [m]	Y (p.N) [m]	Z (p.N) [m]
000_000	rejected							
000_001		0.8005	0.5993	0.0022	0.006	318.017	811.629	3.184
000_002		0.7915	0.6111	–0.0043	0.006	321.966	806.449	3.116
000_003		0.7938	0.6082	0.0005	0.007	326.010	801.185	3.051
000_004	rejected							
001_000	rejected							
001_001		0.7996	0.6004	0.0113	0.010	317.990	811.628	6.000
001_002		0.7911	0.6117	0.0000	0.012	322.009	806.398	6.000
001_003		0.7943	0.6075	0.0016	0.011	325.992	801.193	6.002
001_004	rejected							
002_000	rejected							
002_001		0.8001	0.5997	0.0116	0.010	318.039	811.488	9.522
002_002		0.7837	0.6209	0.0143	0.020	321.992	806.382	9.996
002_003		0.7951	0.6064	0.0068	0.012	325.995	801.176	10.002
002_004	rejected							
003_000	no data							
003_001	rejected							
003_002	roof	0.7848	0.6193	–0.0238	0.022	322.119	806.258	12.939
003_003	roof	0.7915	0.6106	–0.0267	0.017	325.841	801.424	12.760
entire wall		0.7930	0.6093	0.0027	0.029	321.962	806.443	7.718
fragment		0.7918	0.6108	0.0034	0.019	322.127	806.231	6.186
fragment _sor		0.7918	0.6108	0.0034	0.019	322.122	806.238	6.185

cleaned with the SOR filter. Out of 19 designated fields, 8 were rejected. The rejected fields were located on the edges of the object. For 11 analyzed fields, RMS values not exceeding 0.025;m were obtained, while for the entire point cloud, the RMS was 0.029;m, and for the designated fragment in both variants, it was 0.019 m. The obtained RMS values are satisfactory, as changes over the centimeter level were expected for the object. In Table 5, the values of normal vectors, root mean square, and coordinates of the centroid for planes fitted into the selected point cloud fragments representing the wall of the building on Stefana Okrzei Street in Warsaw for cycle 2 were summarized. The RMS values did not exceed 0.020;m, except for the analysis of the entire point cloud, for which the RMS was 0.057 m.

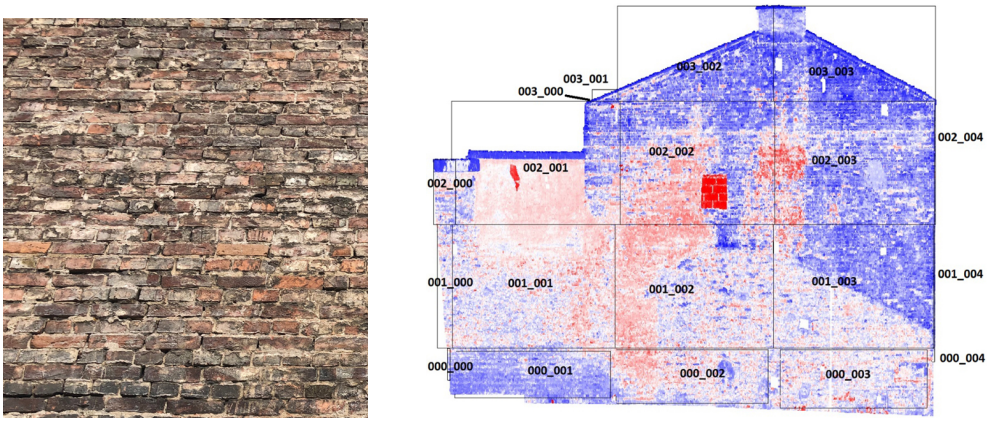

(a) (b)

Fig. 8. Views of the wall of the building on Okrzei Street a) surface structure of the wall, b) view in intensity colors with the division into analyzed areas applied

Table 5. A summary of normal vector values, RMS, and centroid coordinates for planes fitted to the designated point cloud segments representing the wall of the building on Stefana Okrzei Street in Warsaw – Cycle 2

ID	Notes	N_x	N_y	N_z	RMS [m]	X (p.N) [m]	Y (p.N) [m]	Z (p.N) [m]
000_001		0.8006	0.5992	0.0024	0.005	318.014	811.627	3.186
000_002		0.7915	0.6112	–0.0045	0.006	321.969	806.442	3.121
000_003		0.7937	0.6083	–0.0001	0.007	326.011	801.180	3.054
001_001		0.7998	0.6001	0.0119	0.010	317.991	811.618	6.002
001_002		0.7912	0.6116	0.0002	0.012	322.030	806.367	6.000
001_003		0.7945	0.6073	0.0021	0.010	325.988	801.192	6.001
002_001		0.7999	0.6000	0.0109	0.011	318.053	811.462	9.455
002_002		0.7832	0.6216	0.0147	0.019	322.013	806.351	9.998
002_003		0.7953	0.6062	0.0071	0.012	326.001	801.162	10.004
003_002	roof	0.7845	0.6195	–0.0282	0.020	322.079	806.304	12.925
003_003	roof	0.7904	0.6118	–0.0305	0.012	325.856	801.402	12.762
całość		0.7932	0.6090	0.0041	0.057	321.990	806.402	7.324
fragment		0.7916	0.6110	0.0045	0.019	322.121	806.235	6.194
fragment _sor		0.7916	0.6111	0.0045	0.019	322.121	806.236	6.184

Using data from Tables 4 and 5, angles between normal vectors (α_N) and the distances between the initial points of normal vectors $N(s_{N_1-N_2})$ were determined according to previously presented formulas and compiled in Table 6. The maximum change value for a given field was determined based on the following formula (Eq. 3.4):

$$\text{change } N = \text{length of the field diagonal} \cdot \tan \alpha_N + s_{N1-N2} \tag{3.4}$$

In this variant, the RMS average value was purposefully excluded from the calculated change N because the analyzed point clouds were not influenced by vegetation noise.

To evaluate the accuracy of the determined change N, distance values between measurement cycles, as determined by the C2C algorithm, were used. Table 6 illustrates the percentage of points with distances smaller than the determined change N. Fields where the change N was lower than the actual occurring change are highlighted in green. For fields 000_001, 000_002, and 000_003, their rectangular shape and ground-level location proved problematic. A low percentage of agreement was verified for fields 001_003 and 002_003.

The incorrect change value determined for the entire point cloud is marked in blue. This inaccuracy arises from the building's protruding cornices, which distorted the results. It is also noteworthy that a high degree of agreement was achieved for the point cloud segment, both without filtration and with SOR. filtration. This indicates that when it is necessary to show a global change trend, data can be used even for a relatively large area.

Table 6. A summary of the angle between normal vectors, distances between initial points of normal vectors, change values determined based on them, theoretical change, and the agreement between the determined change and the theoretical change for cycles 1 and 2

ID	Notes	Angle N [g]	Distances between the initial points of vectors N [m]	Change N [m]	The percentage of points included in the change [%]
000_001		0.01823	0.004	0.007	11.5
000_002		0.01542	0.009	0.011	25.8
000_003		0.03795	0.006	0.011	25.0
001_001		0.04263	0.010	0.016	81.8
001_002		0.01698	0.037	0.040	99.7
001_003		0.03355	0.004	0.009	9.3
002_001		0.05000	0.073	0.080	98.8
002_002		0.06068	0.037	0.046	99.7
002_003		0.0252	0.015	0.019	42.0
003_002	roof	0.27963	0.063	0.103	99.8
003_003	roof	0.26588	0.027	0.065	99.5
entire wall		0.09368	0.397	0.439	error
fragment		0.07395	0.011	0.044	99.4
fragment _sor		0.07457	0.002	0.036	99.8

In the case of field 002_003, the algorithm accurately identified the changing trend. The difference in distance from the C2C algorithm was primarily due to the brick structure of the measured surface. The captured point cloud was dense enough to represent the brick roughness and the joints between them (Fig. 9).

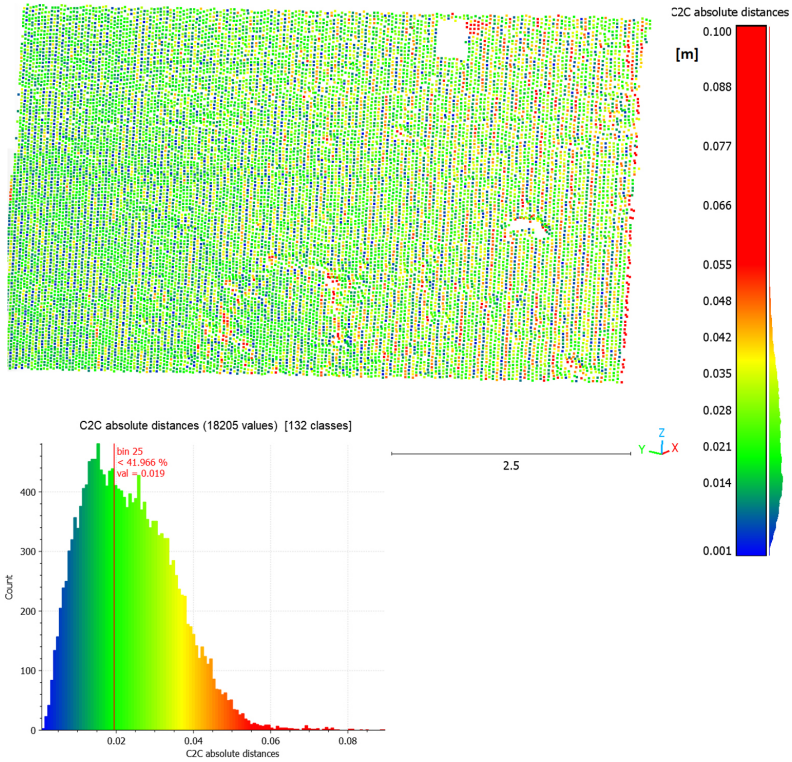

Fig. 9. A color scale map and histogram of distance differences, determined by the C2C algorithm between cycles 1 and 2 for field 002_003 of the building wall on S. Okrzei Street

For field 001_003, a similar situation occurred as in field 001_005 for the dam slope. Despite various challenges, the results obtained for the object demonstrate the considerable potential of the algorithm, while also highlighting the issue of dividing the point cloud into appropriate fields.

4. Conclusions

The research conducted on the experimental structures (the slope and the building wall on Stefana Okrzei Street) underscores the vast potential of applying the algorithm for automatic monitoring using data from various laser scanning sources. Point clouds acquired during monitoring contain a significant amount of data, which makes rapid analysis and identification

of substantial changes in a given area challenging. The proposed algorithm facilitates the quick identification of areas with a high likelihood of change. When a critical value change has been preliminarily identified for a particular field, a detailed comparative analysis can be performed using a point-to-point method. If no change is detected, the data will be archived rather than further processed. This approach considerably reduces data processing time and the required computational power.

Moreover, the determined change values for individual fields can be presented in tabular form or as a color raster. Interpreting such data is much more straightforward than comparing color scale maps that depict distances for millions of points from consecutive measurement cycles. It is worth noting that the choice of color scale can significantly affect the perception of the magnitude and importance of changes occurring on the object. In contrast, numerical comparisons do not present this type of problem.

The presented clustering algorithm requires further research and development. It is essential to develop a detailed accuracy analysis of the obtained results and devise a procedure for cases with high RMS values. The real challenge for the authors is to eliminate situations where small RMS values and underestimated change magnitudes are obtained, as seen in fields 001_005 and 002_005 for the escarpment object and field 001_003 for the object on S. Okrzei Street. This issue is challenging to resolve because fitting a plane to the point cloud relies on the normal distribution of distances, and each time the change on the object will be averaged.

Another crucial aspect is the proper division of the point cloud into fields. Based on previous research, the optimal field shape is square, but due to the irregular shape of real objects, this is often difficult to achieve. Furthermore, the designated fields must not include significant surface breaks, such as cornices. The density of the point cloud, which should be selected based on the expected change size on the object, is also essential. A too dense point cloud will pose a problem for surfaces with high roughness or certain structures, such as a wall made of jointed bricks or stones. In these cases, many measured points will be located in depressions, and as a result of the change on the object, these points will be compared with points measured nearby on the brick/stone surface. A lower point cloud density will minimize such situations.

These challenges are difficult and often solved manually or visually, but they must be addressed to create a reliable automatic monitoring system processing data close to real-time measurements performed after the change.

In subsequent research, the authors plan to test the algorithm on real hydrotechnical facilities: the Klimkówka and Rożnów dams and the stone-surfaced dam in Pilchowice.

Acknowledgements

The presented research is carried out as part of the NCBiR (Polish National Centre of Research and Development) project entitled “Intelligent monitoring system for endangered objects based on automatic non-invasive measurements – IMSGeo” (detailed description can be found on the dedicated website at https://www.gik.pw.edu.pl/zgiisp/Badania-i-nauka/Projekt-POIR 01.01.01-00-0942-21-IMSGeo).

References

[1] M. Scaioni and J. Wang, "Technologies for Dam Deformation Measurement: Recent Trends and Future Challenges", in *Proceedings of 3rd Joint Int. Symp. on Deformation Monitoring*. FIG, 2016, pp. 1–8.

[2] J. Zaczek-Peplinska and M. Kowalska, "Application of non-contactgeodetic measurement techniques in dam monitoring", *Archives of Civil Engineering*, vol. 68, no. 3, pp.49-70, 2022, doi:10.24425/ace.2022.141873.

[3] P. Xiao, R. Zhao, D. Li, Z. Zeng, S. Qi, and X. Yang, "As-built inventory and deformation analysis of a high rockfill dam under construction with terrestrial laser scanning", *Sensors*, vol. 22, no. 2, art. no. 521, 2022, doi: 10.3390/s22020521.

[4] A. Dreier, H. Kuhlmann, and L. Klingbeil, "The potential of UAV-basedLaser Scanning for Deformation Monitoring. Case Study on a Water Dam", in *5th Joint International Symposium on Deformation Monitoring (JISDM 2022)*. Editorial Universitat Politècnica de València, 2023, pp. 261–269, doi: 10.4995/JISDM2022.2022.13833.

[5] S. Zhao, F. Kang, J. Li, and C. Ma, "Structural health monitoring and inspection of dams based on UAV photogrammetry with image 3D reconstruction", *Automation in Construction*, vol. 130, art. no. 103832, 2021, doi: 10.1016/j.autcon.2021.103832.

[6] K. Bakuła, M. Pilarska, A. Salach, and Z. Kurczyński, "Detection of levee damage based on UAS data—Optical imagery and LiDAR pointclouds", *ISPRS International Journal of Geo-Information*, vol. 9, no. 4, 2020, doi: 10.3390/ijgi9040248.

[7] J. Lee, S. Yoo, C. Kim, and H. G. Sohn, "Automatic levee surface extraction from mobile LiDAR data using directional equalization and projection clustering", *International Journal of Applied Earth Observation and Geoinformation*, vol. 116, art. no. 103143, 2023, doi: 10.1016/j.jag.2022.103143.

[8] J. Zaczek-Peplinska and P. Popielski, "Utilisation of terrestrial laser scanning for verification of geometry of numerical models of hydrotechnical structures using the example of a section of the concrete Besko dam", *Czasopismo Techniczne. Środowisko*, vol. 110, no. 1-Ś, pp. 153–164, 2013.

[9] M. Alba, A. Giussani, F. Roncoroni, M. Scaioni, and P. Valgoi, "Geometric modelling of a large dam by terrestrial laser scanning", in *Proceedings of FIG Mondial Congress, Munich, Germany*. FIG, 2006, pp. 8–13.

[10] A. Berberan, I. Ferreira, E. Portela, S. Oliveira, A. Oliveira, and B. Baptista, "Overview on terrestrial laser scanning as a tool for dam surveillance", presented at 6th International Dam Engineering Conference, Lisboa, 2011.

[11] Z. Muszyński and J. Rybak, "Evaluation of terrestrial laser scanner accuracy in the control of hydrotechnical structures", *Studia Geotechnica et Mechanica*, vol. 39, no. 4, pp. 45–57, 2017, doi: 10.1515/sgem-2017-0036.

[12] D. Bolkas, M. O'Banion, J. Prickett, G. Ellsworth, G. Rusek, and H. Corson, "Comparison of TLS and sUAS point clouds for monitoring embankment dams", in *5th Joint International Symposium on Deformation Monitoring (JISDM), 20-22 June 2022, Valencia, Spain*. Universitat Politècnica de València, 2023, doi:10.4995/JISDM2022.2022.13868.

[13] J. Kang, D. Kim, C. Lee, J. Kang, and D. Kim, "Efficiency Study of Combined UAS Photogrammetry and Terrestrial LiDAR in 3D Modeling for Maintenance and Management of Fill Dams", *Remote Sensing*, vol. 15, no. 8, 2023, doi:10.3390/rs15082026.

[14] H. Seo, "Tilt mapping for zigzag-shaped concrete panel in retaining structure using terrestrial laser scanning", *Journal of Civil Structural Health Monitoring*, vol. 11, no. 4, pp. 851–865, 2021, doi: 10.1007/s13349-021-00484-x.

[15] L. Yang, J. C. Cheng, and Q. Wang, "Semi-automated generation of parametric BIM for steel structures based on terrestrial laser scanning data", *Automation in Construction*, vol. 112, art. no. 103037, 2020, doi: 10.1016/j.autcon.2019.103037.

Określanie trendu zmian geometrycznych obiektu hydrotechnicznego w oparciu o dane w postaci chmur punktów LiDAR

Słowa kluczowe: LiDAR, wektor normalny, chmur punktów, naziemny skaning laserowy, deformacje obiektów hydrotechnicznych

Streszczenie:

Monitorowanie stanu technicznego obiektów hydrotechnicznych stanowi kluczowe zadanie dla zapewnienia bezpieczeństwa ich użytkowania. Obejmuje ono zwykle zmienne środowiskowe (np. poziom piętrzenie i temperaturę betonu, wskazania piezometrów) oraz zmienne geometryczne i fizyczne (odkształcenie, pękanie, filtracja, ciśnienie porowe itp.). Wyniki monitoringu mogą by prezentowane w postaci wieloletnich trendów tych zmiennych w czasie, dzięki czemu stanowią ważną informacją dla zarządców obiektów. Badania nad metodami analizy danych z monitoringu geodezyjnego (manualnego i automatycznego) oraz danych z czujników są ważne w kontekście oceny stanu technicznego i bezpieczeństwa obiektów, szczególnie w przypadku danych rejestrowanych z wykorzystaniem nowych technologii pomiarowych. Nowymi technologiami pozyskiwania danych o zmianach powierzchni obiektów są techniki wykorzystujące skanowanie laserowe (LiDAR) z różnych pułapów: naziemne, z pokładów powietrznych statków bezzałogowych (UAV, dronów), satelitarne wykorzystujące sensory rejestrujące dane geoprzestrzenne i wielospektralne. W artykule zaprezentowano algorytm pozwalający na wyznaczanie trendu zmian geometrycznych w oparciu o dane z naziemnego skaningu laserowego zarówno dla powierzchni obiektów betonowych jak i ziemnych. W pracach nad opracowaniem kolejnych kroków postępowania wykorzystano wektory normalne do analizy występowania zmian oraz obliczenia lokalnych kątów nachylenia powierzchni i zmian obiektu. Wektory normalne uzyskiwano poprzez wpasowanie lokalnych płaszczyzna metodą najmniejszych kwadratów w chmurę punktów. W większości zastosowań analizy odkształceń i deformacji powierzchni wykonywane w oparciu o chmury punktów ze skanowania laserowego sprowadzają się do bezpośredniego porównywania metodą Cloud to Cloud (C2C) i generowania trudnych do interpretacji, rozległych map deformacji. Wstępna analiza trendu zachowania obiektu w oparciu o lokalne wektory normalne pozwala na szybkie wykrywanie ewentualnego zagrożenia. Dzięki temu ogranicza się znacząco ilość obliczeń, a w przypadku gdy obiekt nie wykazuje zmian, szczegółowe interpretacje chmur punktów rozpoczyna się dopiero, po wykryciu zmiany na obiekcie wskazanej przez wektory normalne w postaci narastającego trendu wychylenia. Takie podejście może być stosowane zarówno do monitorowania obiektów betonowych jak i ziemnych, przykłady analizy dla różnych typów obiektów zaprezentowano w artykule.

Received: 2023-08-04, Revised: 2023-09-29